THE JOURNAL OF BIOLOGICAL CHEMISTRY VOL. 290, NO. 43, pp. 26021–26032, October 23, 2015

Structural Basis for Antigenic Peptide Recognition and Processing by Endoplasmic Reticulum (ER) Aminopeptidase 2*

Received for publication, August 17, 2015, and in revised form, September 10, 2015 Published, JBC Papers in Press, September 17, 2015, DOI 10.1074/jbc.M115.685909

Anastasia Mpakali, Petros Giastas, Nikolas Mathioudakis, Irene M. Mavridis, Emmanuel Saridakis,[1] and Efstratios Stratikos[2]

From the National Center for Scientific Research Demokritos, Agia Paraskevi, Athens 15310, Greece

Background: ER aminopeptidases generate antigenic peptides, but how they recognize their substrates is unclear.
Results: We solved crystal structures of ERAP2 in complex with a substrate analogue and a peptide product.
Conclusion: The peptides were found trapped inside a large cavity adjacent to the catalytic site.
Significance: Interactions of the substrate with the internal cavity can result in both substrate permissiveness and limited sequence bias.

Endoplasmic reticulum (ER) aminopeptidases process antigenic peptide precursors to generate epitopes for presentation by MHC class I molecules and help shape the antigenic peptide repertoire and cytotoxic T-cell responses. To perform this function, ER aminopeptidases have to recognize and process a vast variety of peptide sequences. To understand how these enzymes recognize substrates, we determined crystal structures of ER aminopeptidase 2 (ERAP2) in complex with a substrate analogue and a peptidic product to 2.5 and 2.7 Å, respectively, and compared them to the apo-form structure determined to 3.0 Å. The peptides were found within the internal cavity of the enzyme with no direct access to the outside solvent. The substrate analogue extends away from the catalytic center toward the distal end of the internal cavity, making interactions with several shallow pockets along the path. A similar configuration was evident for the peptidic product, although decreasing electron density toward its C terminus indicated progressive disorder. Enzymatic analysis confirmed that visualized interactions can either positively or negatively impact *in vitro* trimming rates. Opportunistic side-chain interactions and lack of deep specificity pockets support a limited-selectivity model for antigenic peptide processing by ERAP2. In contrast to proposed models for the homologous ERAP1, no specific recognition of the peptide C terminus by ERAP2 was evident, consistent with functional differences in length selection and self-activation between these two enzymes. Our results suggest that ERAP2 selects substrates by sequestering them in its internal cavity and allowing opportunistic interactions to determine trimming rates, thus combining substrate permissiveness with sequence bias.

Antigenic peptides presented to immune cells by MHC class I molecules are generated by proteolysis of intracellular proteins (1, 2). A key step in MHC class I peptide optimization is the trimming of N-terminally extended precursors of mature epitopes inside the ER[3] by specialized aminopeptidases such as ER aminopeptidase 1 (ERAP1) and ER aminopeptidase 2 (ERAP2) (3). These enzymes can both generate the correct-length antigenic epitopes as well as destroy them by over-trimming and in this context can regulate the antigenic peptide repertoire, influence cytotoxic immune responses, and help shape epitope immunodominance.

ERAP1 and ERAP2 are highly homologous (50% sequence identity), ER-resident zinc aminopeptidases that along with insulin-regulated aminopeptidase (IRAP) belong to the oxytocinase subfamily of M1-aminopeptidases (4). Of the two, the best studied to date is ERAP1, whose importance for maintaining robust immune responses has been established in several *in vitro* and *in vivo* models (5). ERAP2 has been studied to a lesser degree in part because it lacks a homologue in the mouse hampering *in vivo* studies. ERAP2 has been shown to be able to complement ERAP1-mediated trimming of precursor peptides acting in a concerted manner (6, 7). Accordingly, ERAP2 displays specificity for the N terminus of peptides that is complementary to that of ERAP1 (8, 9). It has been proposed that ERAP1 and ERAP2 form a functional dimer in the ER that optimizes peptide processing (6).

ERAP1 and to a lesser degree ERAP2 are polymorphic. Coding single nucleotide polymorphisms in these enzymes have been repeatedly associated with predisposition to major human diseases (5, 10, 11). Particular ERAP1 and ERAP2 haplotypes have been associated with disease often in epistasis with specific

* This work was supported by the European Union (European Social Fund) and Greek National funds through the Operational Program "Education and Lifelong Learning" of the National Strategic Reference Framework: Research Funding Program of the General Secretariat for Research and Technology Grant ERC-14. This work was also supported by the European Community's Seventh Framework Programme (FP7/2007–2013) under BioStruct-X Grant 283570. The authors declare that they have no conflicts of interest with the contents of this article.

The atomic coordinates and structure factors (codes 5CU5, 5AB2, and 5AB0) have been deposited in the Protein Data Bank (http://wwpdb.org/).

[1] To whom correspondence may be addressed. Tel.: 30-2106503792; E-mail: e.saridakis@inn.demokritos.gr.

[2] To whom correspondence may be addressed. Tel.: 30-2106503918; Fax: 30-2106543526; E-mail: stratos@rrp.demokritos.gr or stratikos@gmail.com.

[3] The abbreviations used are: ER, endoplasmic reticulum; ERAP1 and ERAP2, ER aminopeptidase 1 and 2; IRAP, insulin-regulated aminopeptidase; GPI, glycosylphosphatidylinositol.

MHC alleles and shown to functionally affect antigen processing in model systems (12–17). Two common ERAP2 single nucleotide polymorphisms have been linked with resistance to HIV infection, potentially as a result of balancing selection through host-pathogen interactions (18, 19).

Both ERAP1 and ERAP2 are expected to encounter a highly variable collection of peptide substrates inside the ER. These peptides are initially generated by protein proteolysis in the cytosol and then transported into the ER by the specialized, ATP-dependent, transporter associated with antigen processing (TAP). Many of these peptides are N-terminally extended versions of final antigenic epitopes and need to be processed to generate the mature epitopes (20). Alternatively, over-trimming of ER peptides may result in products too small to bind onto MHC class I, effectively destroying potential epitopes (21, 22). To perform this function, ERAP1 and ERAP2 have to demonstrate significant permissiveness in substrate recognition. Still, their effects on the cellular antigenic peptide repertoire as well as *in vitro* studies have suggested that they possess at least some sequence selectivity (23–27). The first crystal structures of ERAP1 and ERAP2 provided insight on this function (9, 28, 29). Both enzymes form large internal cavities that are located adjacent to their catalytic site and can accommodate large peptides. Interestingly, in the only known conformation of ERAP2 and in one of the two known conformations of ERAP1, this cavity has no access to the external solvent, suggesting obligatory conformational changes so that substrate exchange can take place (9, 29, 30). Indeed, ERAP1 has also been crystallized in a more open conformation in which the internal cavity has direct access to the solvent (28). This conformation has also been speculated for ERAP2 and is expected to facilitate substrate capture and product release (31). Overall, although this internal cavity has been hypothesized to be the binding site for antigenic peptide precursors, the exact mechanisms as well as the structural determinants that underlie substrate recognition and selection remain unclear.

To provide insight on how ERAP2 recognizes epitope precursors, we solved the molecular structures of ERAP2 in complex with a 10-mer substrate analogue and a 9-mer antigenic epitope as well as the ligand-free "apoERAP2" structure. Based on structural and biochemical analysis, we propose a limited-selectivity model for antigenic peptide precursor trimming by ERAP2. According to this model, the peptide is first captured in the enzyme's internal cavity. Inside this limited space, favorable and unfavorable interactions between peptide-side chains with shallow pockets or individual residues lining the cavity stabilize the peptide and cumulatively determine trimming rates. This model can explain experimental observations on the function of both ERAP1 and ERAP2 and accounts both for permissiveness for different substrates as well as for some bias in the sequence of generated antigenic epitopes that may contribute to the generation of complex immunopeptidomes.

Experimental Procedures

Synthetic Peptides—All peptides were purchased from JPT peptide technologies GmbH (Berlin, Germany) and were at >95% purity as judged by reverse-phase HPLC (chromolith C-18 column, Merck). The synthesis and characterization of the DG025 has been described before (32).

Protein Expression and Purification—The expression and purification of recombinant ERAP2 from insect cells has been described before (8, 9). Briefly, ERAP2 was isolated from the supernatant of Hi5 cells (derived from the parental *Trichoplusia ni* cell line, Invitrogen) after infection with recombinant baculovirus harboring the erap2 gene. The supernatant was dialyzed extensively against 10 mM sodium phosphate buffer, pH 8.0, 100 mM NaCl. The dialysate composition was adjusted to 50 mM sodium phosphate, pH 8.0, 300 mM NaCl, 10 mM imidazole and incubated under gentle stirring with nickel-nitrilotriacetic acid (Ni-NTA)-agarose slurry (Bio-Rad). The enzyme was eluted from the Ni-NTA column by washing with increasing concentrations of imidazole-containing buffer. For crystallization, the enzyme was further purified by size-exclusion chromatography using a Sephadex S-200 column equilibrated with 10 mM Hepes buffer, pH 7.0, 100 mM NaCl. During all steps of the purification, enzyme purity was estimated by SDS-PAGE and activity by the L-arginine-7-amido-4-methylcoumarine assay (8).

Enzymatic Assays—Enzymatic activity was followed by the hydrolysis of the model fluorigenic substrate the L-arginine-7-amido-4-methylcoumarine as previously described (8). Measurements were performed on a TECAN infinite M200 microplate fluorescence reader and on a QuantaMaster 4 spectrofluorimeter (Photon Technology International, Birmingham, NJ). For analysis of the trimming rates of model peptides (alanine scan), 20 μM concentrations of peptide were incubated with 5 nM ERAP2 in 50 mM Hepes, pH 7.0, 100 mM NaCl for 15 min at room temperature, and the reaction was stopped by flash-freezing. Trimming products were analyzed by reverse-phase HPLC on a chromolith C-18 column (Merck) equilibrated in 10 mM sodium phosphate buffer, pH 6.8, and 10% acetonitrile using a 10–50% acetonitrile gradient. Elution was monitored at 257 nm. The area under the peak corresponding to each substrate was integrated and used to calculate the trimming rate. For the LG_nL series of peptides, 20 μM concentrations of each peptide were incubated with 250 nM ERAP2 at 37 °C for 2 h in 50 mM Hepes, pH 7.0, 100 mM NaCl. Reactions were terminated with the addition of 0.25% (v/v) trifluoroacetic acid (TFA). The reactions were analyzed by reverse-phase HPLC on a chromolith C-18 column equilibrated with 0.05% TFA, 10% acetonitrile using a linear gradient to 40% acetonitrile.

Crystallization, Data Collection, and Structure Determination—ERAP2 was crystallized using conditions very similar to those previously reported (9, 33, 34) adapted from conditions found in the Morpheus protein crystallization screen (Molecular Dimensions Ltd. and Ref. 35) using the vapor diffusion hanging drop technique.

ApoERAP2—Purified ERAP2 was incubated at 4 °C with 10 mM EDTA for 12–16 h before crystallization. The crystal used for data collection was obtained at 4 °C by mixing 1 μl of ERAP2 stock solution (6 mg/ml protein in 150 mM sodium chloride and 25 mM HEPES at pH 7.0) with 1 μl of reservoir condition (7% (w/v) PEG of mean M_r 8000, 20% (v/v) ethylene glycol, 69 mM MES, and 31 mM imidazole at pH 6.5). X-ray diffraction data

were collected at 100 K using synchrotron radiation at the X06DA beamline (Swiss Light Source, Paul Scherrer Institut, Villigen, Switzerland). Diffraction data up to 3.02 Å resolution were processed with MOSFLM and scaled with the SCALA software (36, 37). Five percent of reflections were flagged for R_{free} calculations. The crystal was isomorphous with previously obtained ERAP2 crystals, belonging to space group $P2_1$ with $a = 74.6$ Å, $b = 135.2$ Å, $c = 126.5$ Å, and $\beta = 90.7°$. The structure, containing two molecules per asymmetric unit, was determined by molecular replacement using the ERAP2 coordinates (Protein Data Bank ID 4E36). The PHENIX suite (38) was used for structure refinement, imposing 2-fold non-crystallographic symmetry restraints. Alternating cycles of restrained refinement and manual fitting/building with Coot (39) followed by optimization with PDB_REDO (40) resulted in an R factor and R_{free} of 21.27% and 26.57%, respectively. Besides the two crystallographically independent protein molecules, the asymmetric unit included a total of 20 sugar residues and 193 water molecules. There was no assignable density before residue 54 of chain A and residue 55 of chain B. Also missing are residues 127–129, 503–527, and 572–580 of chain A and 128–131, 503–531, and 571–582 of chain B.

ERAP2 Complexed with Peptide GPI—To generate the complex, the purified protein (6 mg/ml in 150 mM sodium chloride and 25 mM HEPES at pH 7.0) was incubated with 450 μM GPI for 1 h at room temperature. The crystal used for data collection was obtained at 4 °C by mixing 1 μl of complexed protein solution with 1 μl of reservoir condition (7% (w/v) PEG of mean M_r 8000, 20%(v/v) ethylene glycol, 59 mM MES, and 41 mM imidazole at pH 6.3). Data collection up to 2.73 Å resolution, processing, and refinement were performed as described for apoERAP2. The crystal was isomorphous with previously obtained ERAP2 crystals, belonging to space group $P2_1$ with $a = 75.6$ Å, $b = 135.4$ Å, $c = 128.2$ Å, and $\beta = 90.2°$. Alternating cycles of restrained refinement with PHENIX suite and manual fitting/building with Coot were performed, reaching an R factor and R_{free} of 22.28% and 28.59%, respectively. Besides the two crystallographically independent protein molecules, the asymmetric unit includes a total of 29 sugar residues and 102 water molecules. There was no assignable density before residue 54 of chain A and chain B. Also missing are residues 503–514 of chain A and 503–531 of chain B.

ERAP2 Complexed with Peptide Analogue DG025—Purified ERAP2 (1 mg/ml in 150 mM sodium chloride and 25 mM HEPES at pH 7.0) was incubated with 80 μM DG025 ligand for 1 h at room temperature, and then the mixture was concentrated at 4 °C to 6 mg/ml using a Centricon-10. The crystal used for data collection was obtained at 4 °C by mixing 1 μl of complexed protein solution with 1 μl of reservoir condition (6%(w/v) PEG of mean M_r 8000, 25%(v/v) ethylene glycol, 59 mM MES, and 41 mM imidazole at pH 6.3). The drop was incubated for 7.5 h over that reservoir and then transferred over a reservoir at lower PEG concentration (4% (w/v)) for slow growth, as described in Saridakis and Chayen (41). Data collection up to 2.5 Å resolution, processing, and refinement were performed as described above. This crystal was also isomorphous with the above, belonging to space group $P2_1$ with $a = 75.4$ Å, $b = 134.4$ Å, $c = 129.0$ Å, and $\beta = 90.5°$. The structure, containing two molecules per asymmetric unit (chains A and C), was determined by molecular replacement using the ERAP2 coordinates (Protein Data Bank ID 4E36). Alternating cycles of restrained refinement and manual fitting/building with Coot were performed, reaching an R factor and R_{free} of 19.81% and 25.80%, respectively. Besides the two crystallographically independent protein molecules, the asymmetric unit includes a total of 27 sugar residues and 403 water molecules. There was no assignable density before residue 54. Also missing are residues 502–528 of chain C.

Results

Structures of ApoERAP2 and ERAP2 with Bound Peptide Ligands—To gain insight onto peptide recognition by ERAP2, we co-crystallized ERAP2 with the transition-state peptide analogue DG025 (hPhe-Ψ{PO_2CH_2}-LKHHAFSFK-NH_2, where hPhe stands for homophenylalanine and ψ for the pseudopeptide bond) that is designed as a model precursor based on the antigenic epitope SRHHAFSFR from the aggrecan protein normally presented by the HLA-B*27:05 MHC class I allele. We also crystallized ERAP2 with the antigenic epitope GPI (full sequence GPGRAFVTI), which is derived from the env protein of the HIV 1 IIIB. The GPI peptide has been reported to be a trimming product of ERAP2, and its precursor peptide sequence RGPGRAFVTI has been reported to be presented by HLA-A2.1 and to induce immune responses (6, 42). The structures were determined to 2.5 and 2.73 Å, respectively (Table 1). The phosphinic group in DG025 mimics the transition state analogue formed during peptidic bond cleavage by zinc aminopeptidases, and as a result DG025 acts as a potent inhibitor with an IC_{50} of 26 nM (Fig. 1). In contrast, the GPI peptide has been shown to require ERAP2 to be produced *in vitro* by an N-terminally extended precursor (6, 43) and, therefore, constitutes a product of ERAP2. Finally, to better understand any conformational rearrangements that occur upon ligand binding we generated an apoERAP2 form in which the Zn(II) atom at the catalytic site was removed by incubating the enzyme with EDTA. This apoERAP2 was crystallized and its structure solved at 3.0 Å and found to be devoid of electron density at the catalytic site (Table 1). Strikingly, catalytic site residues, including residues that normally chelate the Zn(II) atom and residues that stabilize the N terminus of the peptide-ligand, were found in positions identical to previously determined structures of ERAP2 obtained with bound ligands in the active site (9, 33).

Peptides Are Captured in the Internal Cavity with No Direct Access to the External Solvent—All three molecular structures were found in a near-identical configuration to the previously determined ERAP2 structures and correspond to a closed conformation in which the catalytic center of the enzyme is located adjacent to a large internal cavity that has no direct access to the external solvent (9, 33, 34). This conformation is very similar to one of the available structures of ERAP1 (PDB code 2YD0), although ERAP1 has also been crystallized in an open conformation (Fig. 2) (28, 29). The peptidic ligands DG025 and GPI were found trapped inside this cavity with their N terminus positioned at the catalytic center in a canonical orientation as would be expected for catalysis (Fig. 2). The N-terminal moiety of both peptides primarily interacts with residues in domain II

TABLE 1
Crystallographic data and refinement statistics
r.m.s.d., root mean square deviation.

Structure	ApoERAP2	ERAP2-DG025	ERAP2-GPI
PDB entry code	5CU5	5AB0	5AB2
Space group	P 1 2_1 1	P 1 2_1 1	P 1 2_1 1
Cell	74.6 Å	75.4 Å	75.6 Å
	135.2 Å	134.4 Å	135.4 Å
	126.5 Å	129.0 Å	128.2 Å
	90.00°	90.00°	90.00°
	90.74°	90.49°	90.24°
	90.00°	90.00°	90.00°
Data collection			
Temperature	100 K	100 K	100 K
Resolution (Å)	48.56-3.02	65.73-2.50	49.01-2.73
Completeness	99.9% (100)[a]	99.4% (99.5)[a]	99.9% (99.8)[a]
Redundancy	6.2 (6.6)	3.7 (3.6)	6.4 (6.3)
R_{merge}	0.14 (0.969)	0.13 (0.81)	0.091 (0.77)
$I/\sigma(I)$	10.3 (2.0)	6 (1.6)	11.4 (2.0)
Unique reflections	49,363	88,335	68,594
Refinement			
Refinement program	Phenix	Phenix	Phenix
Resolution (Å)	3.02	2.5	2.73
Unique reflections used	49,350	88,334	68,272
R (%)	21.3	19.8	22.3
R_{free} (%)	26.6	25.8	28.6
r.m.s.d. from ideal bond lengths (Å)	0.013	0.009	0.010
	1.587	1.282	1.423
Ramachandran statistics			
Non-Gly/Pro residues in most favored regions	92%	92%	87%
Non-Gly/Pro residues in additionally allowed regions	6%	7%	11%
Non-Gly/Pro residues in disallowed regions	2%	1%	2%

[a] Values in parentheses are for the outermost shell

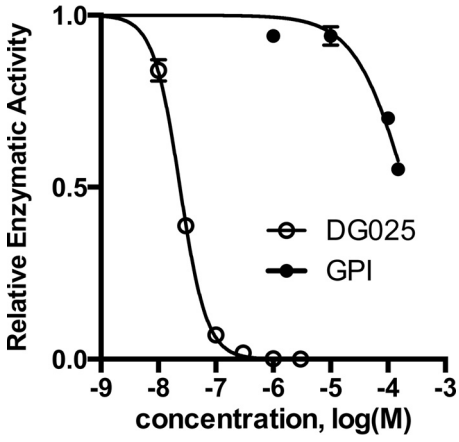

FIGURE 1. **Titration of DG025 and GPI peptides while following the hydrolysis of L-arginine-7-amido-4-methylcoumarine by ERAP2.**

of the enzyme. As the peptide extends away from the active site, however, it makes further interactions with residues from domain IV (Figs. 2 and 3). All 10 residues of DG025 could be built based on available electron density with good confidence (Fig. 3*A*). The same was not the case for GPI as from the nine residues in that peptide GPI only six have been accounted for due to progressive weakening of the electron density moving from the N terminus to the C terminus (Fig. 3*B*). We interpret this as progressive disorder of the peptide presumably reflecting the weak affinity of this product of enzymatic catalysis (Fig. 1). In both cases, there is no apparent opening in the internal cavity of ERAP2 to allow for peptide binding and release, and we, therefore, conclude that both peptides were sequestered by a more open conformation of ERAP2, perhaps similar to the known open conformation of ERAP1 (28, 29).

Interactions between the Peptide Side Chains and ERAP2—The peptide side chains were found to make several interactions with side chains of ERAP2 lining the internal cavity that could be contributing in the stabilization of the binding (Fig. 4*A*). hPhe-1 of DG025 abuts on the hydrophobic S1 specificity pocket making π stacking interactions with Phe-450 as previously described for a phosphinic pseudopeptide inhibitor (33). Lys-3 and His-4 were found inserted in a hydrophobic pocket between Tyr-455 and Tyr-892, possibly stabilized by π stacking interactions between His-4 and these two aromatic residues (44). His-5 abuts to Arg-345 and Phe-7 abuts to Trp-364 in configurations that imply stabilizing π-stacking interactions. Phe-9 was found buried in a hydrophobic pocket formed by Leu-858 and Leu-825 in its bottom and Asn-854 and Asn-822 at its entrance. Finally, the aliphatic part of Lys-10 interacts with the phenyl ring of Tyr-826, and its free amine faces away from Lys-756 and Lys-792 presumably due to electrostatic repulsive forces. Interestingly, the Lys10 side chain has a slightly different orientation in the other monomer of the crystallographic ERAP2 dimer, approaching Tyr-416 within hydrogen-bonding distance.

Two side chains of GPI make clear interactions with cavity residues (Fig. 4*B*). Arg-4 is located in between Tyr-455 and Tyr-892, and Phe-7 makes π-stacking interactions with Trp-364. Similar interactions are observed also in the ERAP2-DG025 structure, suggesting conservation on the use of specificity pockets. Interestingly, based on the electron density interpreted to belong to GPI, two distinct backbone configurations were built for this peptide around residues 3 and 4, which, however, position Arg-4 in the same pocket (between Tyr-455 and Tyr-892). This finding implies some conformational heterogeneity for GPI, which is also consistent with

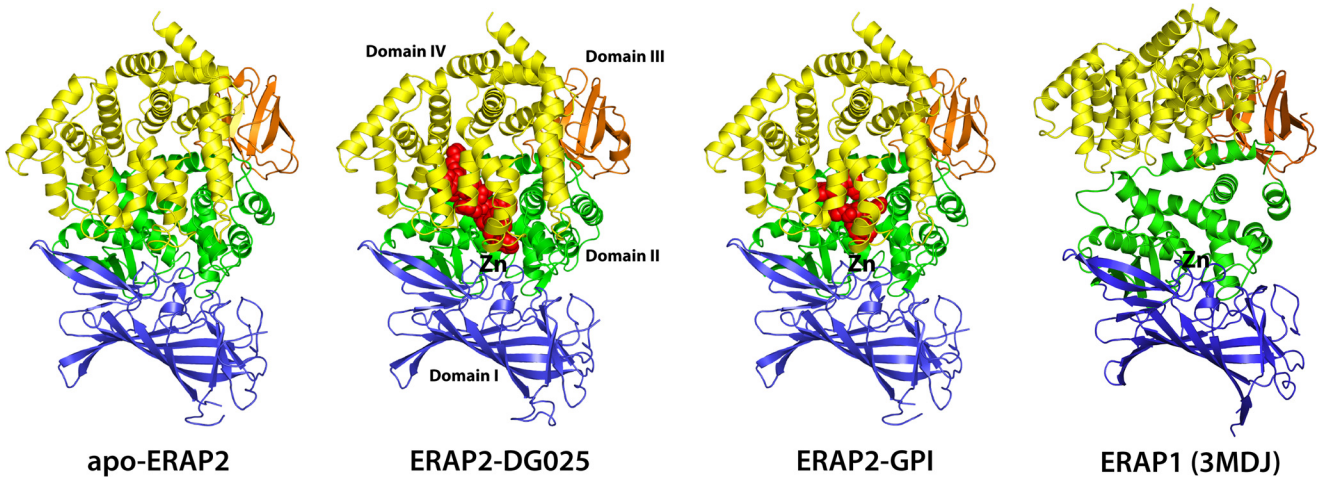

FIGURE 2. **Schematic representations of determined crystal structures of ERAP2 colored by domain.** The DG025 substrate analogue and the GPI peptide epitope are shown in *red spheres*. The catalytic site Zn(II) atom location is indicated. The structure of the open conformation of ERAP1 (PDB code = 3MDJ) is shown for comparison.

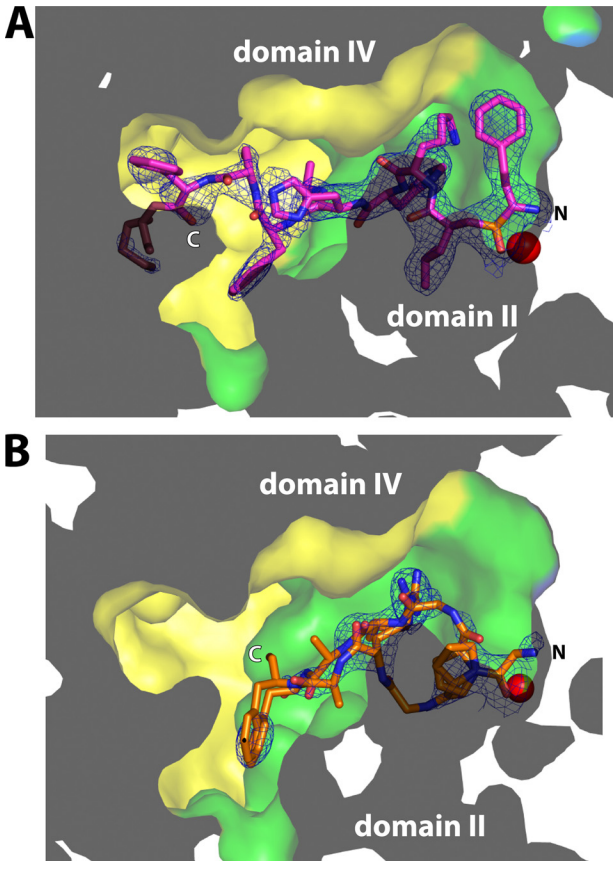

FIGURE 3. **Cutaway view of the ERAP2 internal cavity in surface representation with complexed ligands shown in stick representation (*panel A*, substrate analogue DG025 is in *magenta*; *panel B*, GPI epitope is in *orange*).** The catalytic site Zn(II) atom is shown as a *red sphere*. The N and C termini of each peptide are indicated by the letter N and C, respectively. The peptides are located inside a cavity defined by domain II (in *green*) and domain IV (in *yellow*). The refined $2F_o - F_c$ electron density map is shown as a *blue mesh*.

the lack of electron density for the C-terminal moiety of the peptide.

Overall, the substrate analogue DG025 was found to be well ordered throughout the sequence and to make several interactions with pockets in the ERAP2 internal cavity. In contrast, the product GPI was found to be partially disordered and to make fewer interactions, possibly consistent with the weaker recognition of a product of catalysis that needs to be released before the next catalytic cycle. Interestingly, both peptides utilize the pocket between Tyr-455 and Tyr-892 as an S3′ specificity pocket. In contrast, in a previously reported molecular structure of ERAP2 with an inhibitor, the pocket between Tyr-455 and Tyr-892 was utilized by the third residue of the pseudopeptide inhibitor, thus constituting the S2′ specificity pocket of the enzyme. This suggests that depending on the peptide sequence, the substrate conformation can vary, leading to different binding registers for different peptides.

Conformational Changes upon Ligand Binding—Comparison of the apoERAP2 structure to the ERAP2-DG025 and ERAP2-GPI complexes revealed two main structural reconfigurations related to ligand binding: (*a*) re-orientation of the side chain of the catalytic center Tyr-455 and (*b*) a lateral displacement of the 444–454 strand that contains the residue Phe-450 that helps define the S1 pocket of the enzyme. These changes are described in detail below.

ERAP2 contains a catalytic Tyr residue (Tyr-455) that can stabilize the transition state during catalysis (9). The equivalent residue in ERAP1, Tyr-435, has been suggested to be part of a structural switch that regulates the enzymatic activity of open and closed conformation states (28). In previously analyzed structures of ERAP2, Tyr-455 was found in a configuration identical to the one found in the closed conformation of ERAP1, consistent with the overall closed conformation of ERAP2 (9, 33, 34). This finding supported the hypothesis that the configuration of Tyr-455 is linked to the overall conformation of the enzyme and is part of a conformational switch that limits the activity of open conformations. Comparing our three structures to known structures of ERAP1 and ERAP2, we find that Tyr-455 is oriented toward the active site in both structures with peptides (DG025 and GPI) consistent with an active enzyme. In contrast, in the apoERAP2 structure (to our knowledge the first ERAP2 structure obtained devoid of any ligand in the active site), Tyr-455 is oriented away from the zinc atom and has a configuration closer to that of the equivalent Tyr

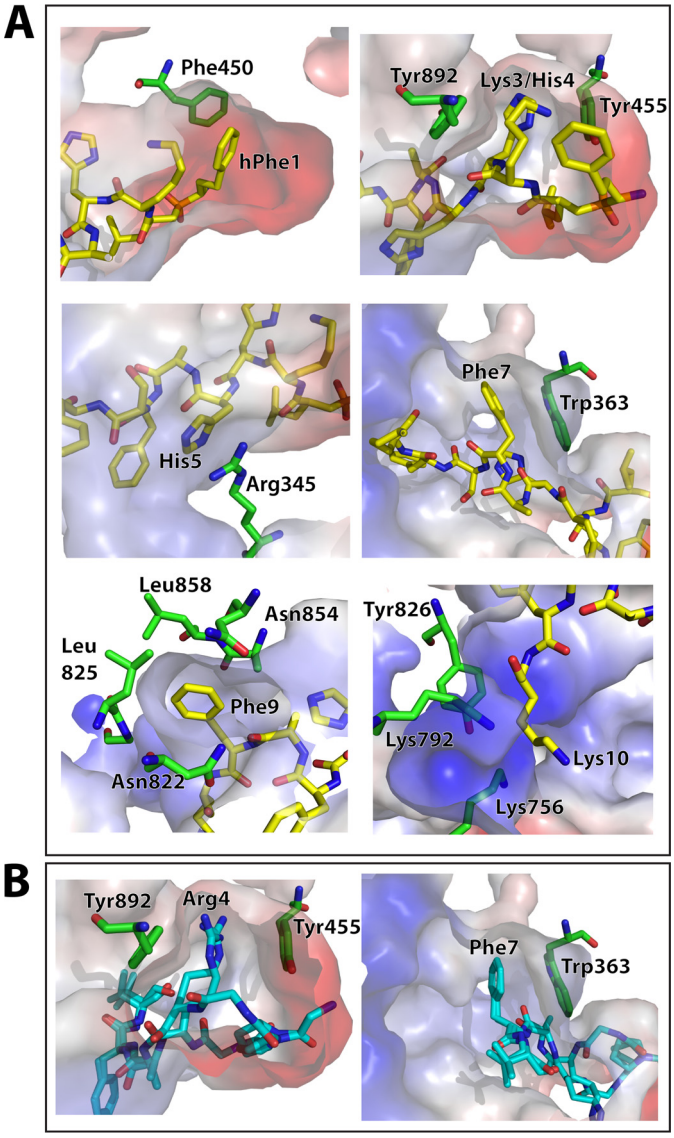

FIGURE 4. **Major interactions between the bound ligands and ERAP2 side chains.** *Panel A*, interactions between DG025 (*yellow sticks*) and ERAP2. *Panel B*, interactions between GPI (*cyan sticks*) and ERAP2. The ERAP2 substrate cavity is shown in surface representation colored by electrostatic potential (*red* = negative, *blue* = positive, *white* = neutral). ERAP2 side chains are shown in *green sticks*. The peptide ligand is oriented so that its N terminus is located toward the *right* and its C terminus toward the *left*, similar to the orientation in Fig. 3.

found in the inactive conformation of ERAP1 (Fig. 5*A*). This finding suggests that in ERAP2 the orientation of the catalytic Tyr-455 depends on the presence of ligand and not only on the overall protein conformation as suggested for the equivalent residue in ERAP1. Whether the link between the orientation of this residue and the overall protein conformation is a unique characteristic of ERAP1 that is missing in ERAP2 cannot be determined at this point as we lack structural information for open conformations of ERAP2.

Phe-450 is a conserved residue in the oxytocinase subfamily of M1 aminopeptidases and lines the side of the S1 specificity pocket, making important interactions with substrates (8, 33). Aligning all known ERAP2 structures revealed that the strand between residues 444 and 454 is shifted in the apoERAP2 structure compared with the ligand-containing ERAP2 structures (Fig. 5*B*). This conformational adjustment appears to define a limited induced fit that helps better accommodate the substrate. Interestingly, the equivalent residue (Phe-450) and surrounding region is disordered in the open conformations of ERAP1 and considered to be a key component of the active conformation of that enzyme (28, 29). The finding that this region is responsive to ligand binding in ERAP2 suggests that it may be a conserved ligand recognition feature in this family of aminopeptidases.

Comparison of Peptide Configuration in ERAP2 and IRAP—IRAP is a highly homologous enzyme to ERAP2 (50% sequence identity) that specializes in generating antigenic peptides for cross-presentation by dendritic cells. We recently determined the crystal structure of IRAP in the presence and absence of the peptide analogue DG025 (32). In those structures, IRAP was found in a semi-closed conformation in between the known conformations of ERAP1 and ERAP2. Similar to the ERAP2-DG025 structure presented here, the DG025 peptide was found to extend away from the catalytic center of IRAP, toward the distal end of the internal cavity and make interactions with both domains II and IV. To gain insight on how the same peptide may be recognized by these two aminopeptidases, we compared the configuration of DG025 after aligning the catalytic centers of the two enzymes (Fig. 6). The configuration of the peptide was near-identical for the first two residues (hPhe-$\Psi\{PO_2CH_2\}$-Leu, where hPhe stands for homophenylalanine and ψ for the pseudopeptide bond) consistent with the canonical orientation required for the scissile bond and adjacent amino acids in order to promote catalysis. Moving toward the C terminus, however, the conformation of DG025 in the two structures is different both in backbone orientation and side-chain interactions with the enzyme. Specifically, in the IRAP structure, His-4 points to the opposite direction compared with His-4 in the ERAP2 structure, presumably due to the lack of the Tyr 455/Tyr-892 pocket in IRAP. Furthermore, the last four amino acids were found in a completely different orientation in the two enzymes. In ERAP2, the peptide adopts an extended configuration, whereas in IRAP it makes a sharp turn after residue 5, and it is lodged between domains II and IV. Interestingly, the interactions between the peptide and IRAP appear less specific and are dominated by general shape complementarity, whereas in ERAP2 some specific side-chain/pocket interactions are visible. This is exemplified by the position of the side chain of Phe-9; no density for this side chain was visible in IRAP, whereas this side chain was well ordered in ERAP2 located within a hydrophobic pocket of the cavity. This phenomenon may be in part due to the more open conformation of IRAP compared with the closed conformation of ERAP2. By comparing these two structures we conclude that although the peptide N terminus configuration is highly limited by restrictions imposed by the catalytic site, the C-terminal moiety of the peptide is free to explore the shape and physicochemical characteristics of the internal cavity of the enzyme to find the best available interactions.

Effects of Side-chain Interactions on Rate of Hydrolysis—The nature of interactions between the side chains of DG025 and ERAP2 suggest that they can affect peptide binding and as a

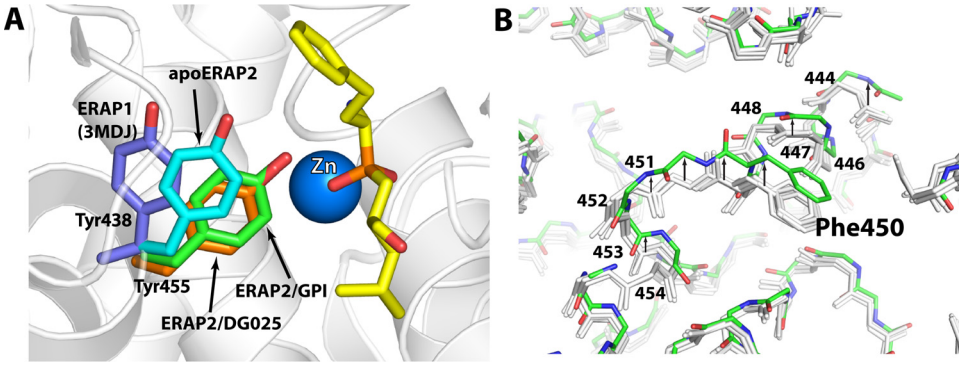

FIGURE 5. **Conformational changes upon ligand binding.** *Panel A*, the ERAP2 tyrosine switch. The relative location of Tyr-455 of ERAP2 in the three crystal structures is shown and compared with the location of the equivalent residue (Tyr-438) in the open/inactive conformation of ERAP1 (from PDB code 3MDJ). The two first residues of DG025 are shown in *yellow sticks*. *Panel B*, shift in the region 444–454 upon ligand binding displaces Phe-450, a key residue for the formation of the S1 pocket. The apoERAP2 is shown in *green sticks*, ERAP2-DG025, ERAP2-GPI, ERAP2 with Lys/MES (PDB code 3SE6), and ERAP2 with inhibitor (PDB code 4JBS) are shown in *light gray*.

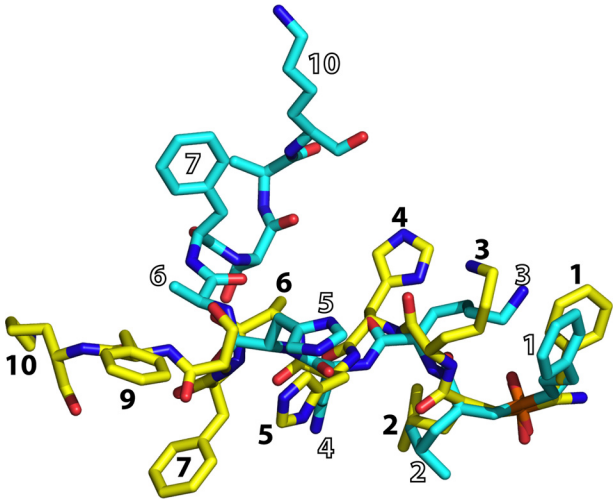

FIGURE 6. **Comparison of the configuration of DG025 bound in ERAP2 (*yellow sticks*) and IRAP (*cyan sticks*).** Numbering is from the N terminus to the C terminus.

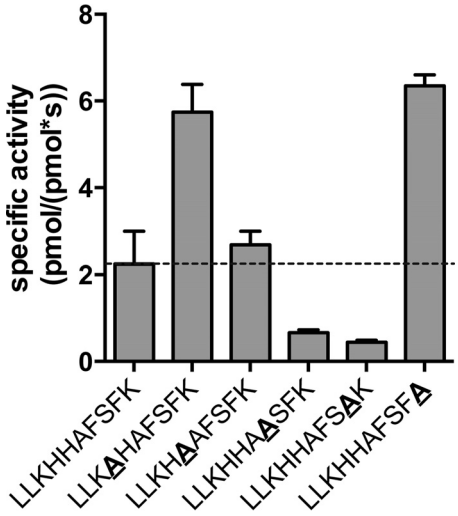

FIGURE 7. **Effect of substituting side chains on the trimming rate of the N-terminal leucine of peptide LLKHHAFSFK by ERAP2.** The *dotted line* is drawn to indicate trimming rate for the control peptide. Substitutions are indicated in *bold letters*.

result the rate of hydrolysis of the N-terminal residue. To further explore this, we determined the rate of hydrolysis of model peptides based on the DG025 sequence in which each residue that made a significant interaction in the ERAP2-DG025 structure was individually mutated to an alanine, allowing us to estimate the effect of the particular side chain to the trimming rate of the N-terminal amino acid (Fig. 7). Interestingly, this alanine scanning revealed that each of the substituted side chains had distinct effects on trimming rates. Specifically, substitution of residues Phe-7 and Phe-9 resulted in significantly lower trimming rates, consistent with a positive role in peptide recognition as suggested by the nature and extent of interactions with the ERAP2 internal cavity (refer to Fig. 4*A*). In contrast, substitution of His-4 and Lys-10 with an alanine led to peptides that were trimmed faster, consistent with a negative impact of those side chains to substrate recognition. This is largely consistent with our structural analysis as His-4 is located in a deep relatively hydrophobic pocket, and Lys-10 is located near two ERAP2 lysine residues that would be expected to make repulsive electrostatic interactions. Finally, substitution of His-5 had no effect, possibly representing a balance between the favorable π stacking interactions with Arg-345 and the unfavorable electrostatic interactions with the same residue. Overall, the combination of structural and enzymatic analysis indicates that trimming rates are influenced by a balance of unfavorable and favorable interactions that are available to the peptide within the limited space of the enzyme's internal cavity.

The Exon 10 Loop Is Structured and Contains a Disulfide Bond—ERAP2 as well as ERAP1 are retained in the ER, although they do not possess any classical ER retention signal. As a result, it has been hypothesized that they are retained through the interaction with other ER resident proteins (4). In ERAP1, a 23-amino acid sequence encoded by exon10 of the gene and predicted to be unstructured was initially implicated in that function (45). Recently, Erp44, an ER resident protein disulfide isomerase, has been shown to retain ERAP1 inside the ER through the formation of a mixed disulfide bond with a cysteine residue in the exon 10 loop (46). This interaction was shown to be important for regulating ERAP1 retention and secretion and in that context controlling blood pressure through angiotensin II cleavage (46). ERAP2 also contains a loop at that location in the structure that may have the same function as in ERAP1. Strikingly, although at least 7 crystal

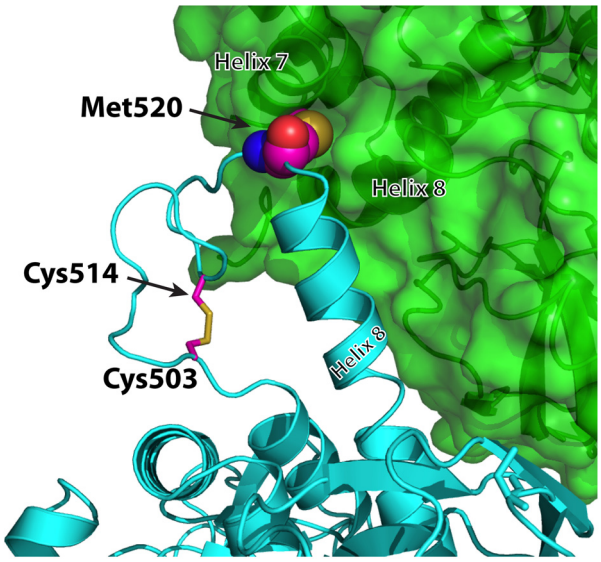


```
ERAP2    SYRNAKNDDLWSSLSNSCLESDFTSGGVCHSDPKMTSNMLAFLGENAEVKEMMTTWTLQK
ERAP1    SYKNTKNEDLWDSMASICPTDGVKGMDGFCSRSQHSSSSSSHWHQEGVDVKTMMNTWTLQK
IRAP     SYASIQSDDLWDSFNEV-------------------------TNQTLDVKRMMKTWTLQK
         ** . :.:***.*: .                          :  :** **.******
```

FIGURE 8. **Schematic representation of exon10 encoded loop of ERAP2 as built on the ERAP2-DG025 crystal structure.** The disulfide bond between Cys-503 and Cys-514 is indicated by *sticks*. Met-520 (shown in *spheres*) inserts in a hydrophobic pocket between helix7 and helix8 of an adjacent ERAP2 molecule in the crystal. A sequence alignment showing a lack of conservation in that region between ERAP2 and the homologous enzymes ERAP1 and IRAP is also shown. The cysteine residues in the loop are indicated in *bold*.

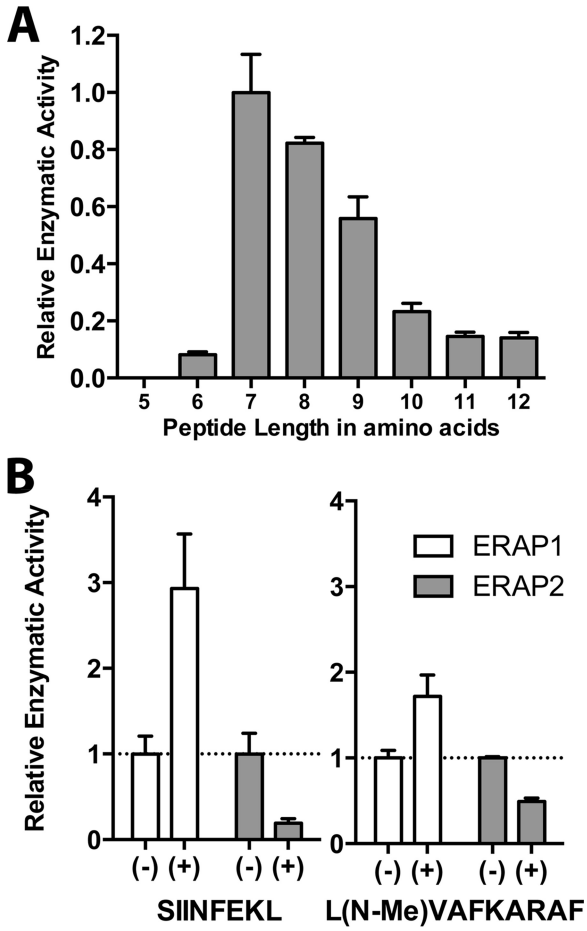

FIGURE 9. **Functional differences between ERAP1 and ERAP2.** *Panel A*, trimming rates for the LG_nL series of peptides. *Panel B*, effect of bystander peptide on the hydrolysis of a small substrate by ERAP1 or ERAP2. The rate of hydrolysis of fluorigenic substrates L-lysine-7-amido-4-methylcoumarine (for ERAP1) and L-arginine-7-amido-4-methylcoumarine (for ERAP2) was determined in the absence or presence of 100 μM SIINFEKL or L(N-Me)VAFKARAF peptide. ERAP1 activity was enhanced in the presence of peptides, whereas ERAP2 was inhibited.

structures of ERAP1 and ERAP2 have been published, this exon 10 loop was not visible in any of them and has been considered disordered. To our surprise, this loop was clearly visible in one monomer of the ERAP2-DG025 structure (Fig. 8). This may be due to the higher resolution of this crystal structure. The loop forms an appendix extending from helix 8 of domain II of ERAP2 and is stabilized through a disulfide bond between Cys-503 and Cys-514. The loop is stabilized in the crystal by another ERAP2 monomer in the lattice. The most prominent interaction involves Met-520 that inserts into a hydrophobic pocket between helix7 and helix8 of an adjacent ERAP2 molecule in the crystal. Because a solvent-accessible disulfide bond stabilizes this loop, it is possible that its structural integrity is regulated by the redox potential of the solvent or interactions with disulfide isomerases. Indeed, although the exon 10 sequence is not conserved in ERAP1 (Fig. 8) the positions of the two cysteine residues are highly similar, suggesting that a similar disulfide bond may be forming in ERAP1. The configuration of this loop may be a structural template that facilitates interactions between ERAP2 or ERAP1 and other proteins in the ER in order to regulate retention and extracellular functions in the context of blood pressure regulation or innate immune responses (46, 47).

ERAP2 Does Not Clearly Recognize the C Terminus of the Peptide and Has Mechanistic Differences from ERAP1—It has been previously proposed that ERAP1 displays a preference for longer peptides by utilizing an allosteric self-regulatory site that recognizes the peptide C terminus (28, 48). This site was later proposed to lie within domain IV of the enzyme (49). Inspection of either the ERAP2-DG025 or ERAP2-GPI structure, however, revealed no strong interactions between ERAP2 and the C terminus of the peptide. This prompted us to investigate whether ERAP2 displays different properties compared with ERAP1 in terms of peptide recognition. We first evaluated the length selection of ERAP2 using a series of peptides of length between 5 and 12 amino acids that carry the motif LG_nL where $n = 3–12$. This series has been used before to demonstrate the length selection of ERAP1 in a sequence-unbiased manner (28, 30). ERAP2 displayed the fastest kinetics for 7-mer peptides and a reduced trimming rate for peptides larger than 10 amino acids (Fig. 9). This is in sharp contrast to the motif observed for ERAP1 that showed faster trimming for peptides longer than 10 amino acids (28). This finding indicates a major mechanistic difference between ERAP1 and ERAP2 and suggests that ERAP2 may be better suited for antigenic peptide destruction rather than generation. Still, because MHC class I binding can protect antigenic peptides from over-trimming and ERAP2 still has appreciable activity for long peptides, it is possible that even this length preference can contribute to the generation of some epitopes (50).

In addition, we compared the ability of ERAP2 to be activated by peptides when trimming a small dipeptidic substrate. This property has been demonstrated for ERAP1 in the context of self-activation for larger peptides (27, 28). We tested two peptides previously shown to activate ERAP1: the ovalbumin epitope SIINFEKL and the non-hydrolysable analogue L(N-Me)VAFKARAF (28). Both peptides activated ERAP1 but failed to show any activation and rather showed inhibition of ERAP2 (Fig. 9). Because SIINFEKL is a product of antigenic peptide precursor trimming and L(N-Me)VAFKARAF is a non-hydrolysable product, inhibition is the expected behavior due to competition with the substrate for the same catalytic site. Lack of activation for ERAP2 indicates that the allosteric activation mechanism proposed for ERAP1 is absent in ERAP2. This is consistent with lack of specific recognition of the peptide C terminus. These mechanistic differences between ERAP1 and ERAP2 may have to be evaluated in the context of distinct biological roles in antigen processing.

Discussion

ER aminopeptidases that trim antigenic peptide precursors have to deal with two aspects of substrate recognition that differentiate them from other aminopeptidases. First, they have to be able to effectively process long peptides. Second, they have to be able to process thousands of different peptide sequences. At the same time the peptide trimming activity in the ER has to be restricted, otherwise all potential antigenic epitopes may be destroyed. This may be in sharp contrast to the cytosol, where aminopeptidases can completely degrade peptides for recycling or other metabolic reasons.

The structural and enzymatic analyses described here suggest a possible mechanism used by ERAP2 to achieve this function. The enzyme contains a large cavity adjacent to the catalytic center that can accommodate large peptides. The first two amino acids of the peptide can occupy the catalytic site in canonical orientation, and the remaining amino acids can extend throughout this cavity making opportunistic interactions with pockets and side chains along the internal lining of the cavity. As a result, the exact configuration of the peptide may depend on its sequence and the propensity of its amino acids to interact with residues in the cavity. The substrate affinity will depend on the efficacy of those interactions. Some sequence bias may exist, but plenty of opportunities exist to accommodate many peptide lengths and sequences. In this manner the enzyme achieves permissiveness while retaining some selectivity. Interestingly, our enzymatic analysis suggests that some interactions may actually confer a negative effect on trimming rates, and thus the requirement for correct N terminus positioning may override optimal side-chain accommodation for the remaining of the peptide. Although this model of substrate recognition well serves the biological function of this enzyme, it makes defining clear sequence-preference motifs difficult until all the major interactions between putative substrates and the internal cavity are mapped with accuracy.

All ERAP2 structures have been found in a closed conformation in which the cavity and catalytic site have no direct access to the external solvent, making substrate capture and product release impossible without a major conformational change. The homologous ERAP1 has, however, been crystallized in open conformations (28, 29) that should also be accessible to ERAP2. Such conformational changes would be necessary for isolating the peptide substrate and to allow for extensive interactions with specificity pockets in the cavity. This mechanism can enhance trimming of larger peptides, as after initial capture the entropic penalty for binding within the closed cavity may be smaller than for an exposed elongated cavity. Furthermore, the isolation of the catalytic site from the solvent could help limit the overall aminopeptidase activity in the ER and, therefore, limit antigen destruction.

It is possible that a similar trimming model applies for the homologous ERAP1, as it also carries a similar internal cavity adjacent to the catalytic center. The shape and physicochemical characteristics of the two cavities are, however, distinct, suggesting that they may confer different interactions with peptide substrates and, therefore, different selectivity (9). Our analysis however, suggests that the two enzymes have additional differences in mechanism. Functional studies have suggested that ERAP1 has a preference for longer peptides (>9-mers) and can be activated by small peptides. These properties have been associated with the ERAP1 ability to recognize the C terminus of long peptides and self-activate (28). Our own analysis of ERAP2, however, suggests that these two properties are not fully shared between the two enzymes. ERAP2 is not activated by peptides and prefers to trim 7-mers, whereas no structural evidence was found, pointing to peptide C terminus recognition. It is possible that mechanistic differences underlie a separate biological role. Indeed, ERAP2 has been proposed to act as a secondary, accessory aminopeptidase to the dominant trimming function of ERAP1. It is conceivable that ERAP2 may function in extending ERAP1 trimming to a wider array of sequences and perform over-trimming for epitope destruction. This observation may be especially relevant to efforts to translate immunology experiments from rodents to humans. Rodents do not express ERAP2, and therefore, it is possible that antigen generation in the ER is significantly different compared with humans.

Previous studies using the mouse homologue of ERAP1 (ERAAP) have suggested that ERAP1 may be able to trim antigenic peptides while bound onto MHC class I molecules (51, 52). This model, by definition, shifts the burden of substrate selection to the MHC and away from ERAP1. At the same time it has been proposed the MHC class I binding can protect peptides from ERAP1 hydrolysis (50, 53). Although no similar experiments have been performed for ERAP2, all known ERAP1 and ERAP2 structures, including the ones presented here, are not consistent with an "onto-MHC" peptide trimming model both due to the limited access to the catalytic site as well as the necessary topology of binding so that scissile bond catalysis can take place (31). Still, ERAP1, and more recently IRAP (32), have been crystallized in more open conformations, and long antigenic peptide precursors are known to weakly interact with MHC. As a result, such a model may be conceivable for some extended peptide precursors. Still, the structures presented here are largely sufficient to explain both the substrate permissiveness of ERAP2 as well as limited selectivity that could influence the antigenic peptide repertoire as observed in

cellular and *in vivo* experiments. Length selection may also arise from competition between ERAP2 and the MHC for peptides depending on peptide affinity and binding kinetics for each binding site.

Our analysis of the ERAP2-DG025 structure revealed for the first time the structure of the sequence between helix7 and helix8, encoded by exon10 of the erap2 gene. Although initially predicted to be unstructured, the ERAP2-DG025 structure described here suggests that this region can fold as an extension of helix8 and be stabilized by a disulfide bond. The equivalent region in ERAP1 has been linked to interactions with the disulfide isomerase ERp44 and it has been suggested that this interaction is part of a mechanism that regulates ERAP1 secretion and blood pressure regulation (46). If this region folds similarly in ERAP1, then the structure depicted in Fig. 8 may constitute a template for protein-protein interactions between ERAPs and other ER proteins or between ERAP1 and ERAP2 themselves. Indeed ERAP1 and ERAP2 have been suggested to operate in cooperation by forming a functional dimer whose structure has remained elusive until now (6).

In summary, our results provide a structural framework for understanding peptide-substrate selectivity by ERAP2 and can help explain both the observed permissiveness for fundamentally different peptide sequences as well as preferences between sequences. Our conclusions may also extend to ERAP1, although the observed mechanistic differences between the two enzymes may support specialized biological roles. Further structural analysis of different sequence peptides in complex with ERAP1 and ERAP2 may be necessary to allow the generation of tools for the prediction of epitope precursor processing inside the ER.

Author Contributions—A. M. performed the enzymatic assays, analyzed the data, processed the diffraction data, and solved the crystal structures. P. G. collected and processed diffraction data and solved the crystal structures. Em. S. performed protein crystallization, processed diffraction data, and solved the crystal structures. I. M. M. solved the crystal structures. N. M. helped solve the apoERAP2 crystal structure. E. S. conceived and supervised the project, helped solve the crystal structures, analyzed data, and wrote the paper with input from all authors. All authors have seen and approved the final version of the manuscript.

Acknowledgments—We thank Efthalia Zervoudi for preparing recombinant ERAP2 and for assisting with the crystallization trials, Dr. Spyros Chatziefthimiou and Dr. James Birtley for collecting diffraction data, and Paraskevi Kokkala and Dr. Dimitris Georgiadis for providing the DG025 peptide.

References

1. Lazaro, S., Gamarra, D., and Del Val, M. (2015) Proteolytic enzymes involved in MHC class I antigen processing: A guerrilla army that partners with the proteasome. *Mol. Immunol.* 10.1016/j.molimm.2015.04.014
2. Weimershaus, M., Evnouchidou, I., Saveanu, L., and van Endert, P. (2013) Peptidases trimming MHC class I ligands. *Curr. Opin. Immunol.* **25,** 90–96
3. Evnouchidou, I., Papakyriakou, A., and Stratikos, E. (2009) A new role for Zn(II) aminopeptidases: antigenic peptide generation and destruction. *Curr. Pharm. Des.* **15,** 3656–3670
4. Tsujimoto, M., and Hattori, A. (2005) The oxytocinase subfamily of M1 aminopeptidases. *Biochim. Biophys. Acta* **1751,** 9–18
5. Fruci, D., Romania, P., D'Alicandro, V., and Locatelli, F. (2014) Endoplasmic reticulum aminopeptidase 1 function and its pathogenic role in regulating innate and adaptive immunity in cancer and major histocompatibility complex class I-associated autoimmune diseases. *Tissue Antigens* **84,** 177–186
6. Saveanu, L., Carroll, O., Lindo, V., Del Val, M., Lopez, D., Lepelletier, Y., Greer, F., Schomburg, L., Fruci, D., Niedermann, G., and van Endert, P. M. (2005) Concerted peptide trimming by human ERAP1 and ERAP2 aminopeptidase complexes in the endoplasmic reticulum. *Nat. Immunol.* **6,** 689–697
7. Lorente, E., Barriga, A., Johnstone, C., Mir, C., Jiménez, M., and López, D. (2013) Concerted *in vitro* trimming of viral HLA-B27-restricted ligands by human ERAP1 and ERAP2 aminopeptidases. *PLoS ONE* **8,** e79596
8. Zervoudi, E., Papakyriakou, A., Georgiadou, D., Evnouchidou, I., Gajda, A., Poreba, M., Salvesen, G. S., Drag, M., Hattori, A., Swevers, L., Vourloumis, D., and Stratikos, E. (2011) Probing the S1 specificity pocket of the aminopeptidases that generate antigenic peptides. *Biochem. J.* **435,** 411–420
9. Birtley, J. R., Saridakis, E., Stratikos, E., and Mavridis, I. M. (2012) The crystal structure of human endoplasmic reticulum aminopeptidase 2 reveals the atomic basis for distinct roles in antigen processing. *Biochemistry* **51,** 286–295
10. Stratikos, E., Stamogiannos, A., Zervoudi, E., and Fruci, D. (2014) A role for naturally occurring alleles of endoplasmic reticulum aminopeptidases in tumor immunity and cancer predisposition. *Front. Oncol.* **4,** 363
11. Kenna, T. J., Robinson, P. C., and Haroon, N. (2015) Endoplasmic reticulum aminopeptidases in the pathogenesis of ankylosing spondylitis. *Rheumatology* **54,** 1549–1556
12. Tsui, F. W., Haroon, N., Reveille, J. D., Rahman, P., Chiu, B., Tsui, H. W., and Inman, R. D. (2010) Association of an ERAP1 ERAP2 haplotype with familial ankylosing spondylitis. *Ann. Rheum. Dis.* **69,** 733–736
13. Reeves, E., Colebatch-Bourn, A., Elliott, T., Edwards, C. J., and James, E. (2014) Functionally distinct ERAP1 allotype combinations distinguish individuals with ankylosing spondylitis. *Proc. Natl. Acad. Sci. U.S.A.* **111,** 17594–17599
14. Maksymowych, W. P., Inman, R. D., Gladman, D. D., Reeve, J. P., Pope, A., and Rahman, P. (2009) Association of a specific ERAP1/ARTS1 haplotype with disease susceptibility in ankylosing spondylitis. *Arthritis Rheum.* **60,** 1317–1323
15. Kirino, Y., Bertsias, G., Ishigatsubo, Y., Mizuki, N., Tugal-Tutkun, I., Seyahi, E., Ozyazgan, Y., Sacli, F. S., Erer, B., Inoko, H., Emrence, Z., Cakar, A., Abaci, N., Ustek, D., Satorius, C., Ueda, A., Takeno, M., Kim, Y., Wood, G. M., Ombrello, M. J., Meguro, A., Gül, A., Remmers, E. F., and Kastner, D. L. (2013) Genome-wide association analysis identifies new susceptibility loci for Behcet's disease and epistasis between HLA-B*51 and ERAP1. *Nat. Genet.* **45,** 202–207
16. García-Medel, N., Sanz-Bravo, A., Van Nguyen, D., Galocha, B., Gómez-Molina, P., Martín-Esteban, A., Alvarez-Navarro, C., and de Castro, J. A. (2012) Functional interaction of the ankylosing spondylitis-associated endoplasmic reticulum aminopeptidase 1 polymorphism and HLA-B27 *in vivo*. *Mol. Cell. Proteomics* **11,** 1416–1429
17. Cortes, A., Pulit, S. L., Leo, P. J., Pointon, J. J., Robinson, P. C., Weisman, M. H., Ward, M., Gensler, L. S., Zhou, X., Garchon, H. J., Chiocchia, G., Nossent, J., Lie, B. A., Førre, Ø., Tuomilehto, J., Laiho, K., Bradbury, L. A., Elewaut, D., Burgos-Vargas, R., Stebbings, S., Appleton, L., Farrah, C., Lau, J., Haroon, N., Mulero, J., Blanco, F. J., Gonzalez-Gay, M. A., Lopez-Larrea, C., Bowness, P., Gaffney, K., Gaston, H., Gladman, D. D., Rahman, P., Maksymowych, W. P., Crusius, J. B., van der Horst-Bruinsma, I. E., Valle-Oñate, R., Romero-Sánchez, C., Hansen, I. M., Pimentel-Santos, F. M., Inman, R. D., Martin, J., Breban, M., Wordsworth, B. P., Reveille, J. D., Evans, D. M., de Bakker, P. I., and Brown, M. A. (2015) Major histocompatibility complex associations of ankylosing spondylitis are complex and involve further epistasis with ERAP1. *Nat. Commun.* **6,** 7146
18. Cagliani, R., Riva, S., Biasin, M., Fumagalli, M., Pozzoli, U., Lo Caputo, S., Mazzotta, F., Piacentini, L., Bresolin, N., Clerici, M., and Sironi, M. (2010) Genetic diversity at endoplasmic reticulum aminopeptidases is main-

tained by balancing selection and is associated with natural resistance to HIV-1 infection. *Hum. Mol. Genet.* **19,** 4705–4714
19. Andrés, A. M., Dennis, M. Y., Kretzschmar, W. W., Cannons, J. L., Lee-Lin, S. Q., Hurle, B., NISC Comparative Sequencing Program, Schwartzberg, P. L., Williamson, S. H., Bustamante, C. D., Nielsen, R., Clark, A. G., and Green, E. D. (2010) Balancing selection maintains a form of ERAP2 that undergoes nonsense-mediated decay and affects antigen presentation. *PLoS Genet.* **6,** e1001157
20. Goldberg, A. L., Cascio, P., Saric, T., and Rock, K. L. (2002) The importance of the proteasome and subsequent proteolytic steps in the generation of antigenic peptides. *Mol. Immunol.* **39,** 147–164
21. York, I. A., Chang, S. C., Saric, T., Keys, J. A., Favreau, J. M., Goldberg, A. L., and Rock, K. L. (2002) The ER aminopeptidase ERAP1 enhances or limits antigen presentation by trimming epitopes to 8–9 residues. *Nat. Immunol.* **3,** 1177–1184
22. Seregin, S. S., Rastall, D. P., Evnouchidou, I., Aylsworth, C. F., Quiroga, D., Kamal, R. P., Godbehere-Roosa, S., Blum, C. F., York, I. A., Stratikos, E., and Amalfitano, A. (2013) Endoplasmic reticulum aminopeptidase-1 alleles associated with increased risk of ankylosing spondylitis reduce HLA-B27 mediated presentation of multiple antigens. *Autoimmunity* **46,** 497–508
23. Evnouchidou, I., Momburg, F., Papakyriakou, A., Chroni, A., Leondiadis, L., Chang, S. C., Goldberg, A. L., and Stratikos, E. (2008) The internal sequence of the peptide-substrate determines its N terminus trimming by ERAP1. *PLoS ONE* **3,** e3658
24. Rastall, D. P., Aldhamen, Y. A., Seregin, S. S., Godbehere, S., and Amalfitano, A. (2014) ERAP1 functions override the intrinsic selection of specific antigens as immunodominant peptides, thereby altering the potency of antigen-specific cytolytic and effector memory T-cell responses. *Int. Immunol.* **26,** 685–695
25. Kim, S., Lee, S., Shin, J., Kim, Y., Evnouchidou, I., Kim, D., Kim, Y. K., Kim, Y. E., Ahn, J. H., Riddell, S. R., Stratikos, E., Kim, V. N., and Ahn, K. (2011) Human cytomegalovirus microRNA miR-US4–1 inhibits CD8(+) T cell responses by targeting the aminopeptidase ERAP1. *Nat. Immunol.* **12,** 984–991
26. García-Medel, N., Sanz-Bravo, A., Alvarez-Navarro, C., Gómez-Molina, P., Barnea, E., Marcilla, M., Admon, A., and de Castro, J. A. (2014) Peptide handling by HLA-B27 subtypes influences their biological behavior, association with ankylosing spondylitis and susceptibility to endoplasmic reticulum aminopeptidase 1 (ERAP1). *Mol. Cell. Proteomics* **13,** 3367–3380
27. Evnouchidou, I., Kamal, R. P., Seregin, S. S., Goto, Y., Tsujimoto, M., Hattori, A., Voulgari, P. V., Drosos, A. A., Amalfitano, A., York, I. A., and Stratikos, E. (2011) Coding single nucleotide polymorphisms of endoplasmic reticulum aminopeptidase 1 can affect antigenic peptide generation *in vitro* by influencing basic enzymatic properties of the enzyme. *J. Immunol.* **186,** 1909–1913
28. Nguyen, T. T., Chang, S. C., Evnouchidou, I., York, I. A., Zikos, C., Rock, K. L., Goldberg, A. L., Stratikos, E., and Stern, L. J. (2011) Structural basis for antigenic peptide precursor processing by the endoplasmic reticulum aminopeptidase ERAP1. *Nat. Struct. Mol. Biol.* **18,** 604–613
29. Kochan, G., Krojer, T., Harvey, D., Fischer, R., Chen, L., Vollmar, M., von Delft, F., Kavanagh, K. L., Brown, M. A., Bowness, P., Wordsworth, P., Kessler, B. M., and Oppermann, U. (2011) Crystal structures of the endoplasmic reticulum aminopeptidase-1 (ERAP1) reveal the molecular basis for N-terminal peptide trimming. *Proc. Natl. Acad. Sci. U.S.A.* **108,** 7745–7750
30. Stamogiannos, A., Koumantou, D., Papakyriakou, A., and Stratikos, E. (2015) Effects of polymorphic variation on the mechanism of endoplasmic reticulum aminopeptidase 1. *Mol. Immunol.* **67,** 426–435
31. Stratikos, E., and Stern, L. J. (2013) Antigenic peptide trimming by ER aminopeptidases: insights from structural studies. *Mol. Immunol.* **55,** 212–219
32. Mpakali, A., Saridakis, E., Harlos, K., Zhao, Y., Papakyriakou, A., Kokkala, P., Georgiadis, D., and Stratikos, E. (2015) Crystal structure of insulin-regulated aminopeptidase with bound substrate analogue provides insight on antigenic epitope precursor recognition and processing. *J. Immunol.* **195,** 2842–2851
33. Zervoudi, E., Saridakis, E., Birtley, J. R., Seregin, S. S., Reeves, E., Kokkala, P., Aldhamen, Y. A., Amalfitano, A., Mavridis, I. M., James, E., Georgiadis, D., and Stratikos, E. (2013) Rationally designed inhibitor targeting antigen-trimming aminopeptidases enhances antigen presentation and cytotoxic T-cell responses. *Proc. Natl. Acad. Sci. U. S. A.* **110,** 19890–19895
34. Evnouchidou, I., Birtley, J., Seregin, S., Papakyriakou, A., Zervoudi, E., Samiotaki, M., Panayotou, G., Giastas, P., Petrakis, O., Georgiadis, D., Amalfitano, A., Saridakis, E., Mavridis, I. M., and Stratikos, E. (2012) A common single nucleotide polymorphism in endoplasmic reticulum aminopeptidase 2 induces a specificity switch that leads to altered antigen processing. *J. Immunol.* **189,** 2383–2392
35. Gorrec, F. (2009) The MORPHEUS protein crystallization screen. *J. Appl. Crystallogr.* **42,** 1035–1042
36. Battye, T. G., Kontogiannis, L., Johnson, O., Powell, H. R., and Leslie, A. G. (2011) iMOSFLM: a new graphical interface for diffraction-image processing with MOSFLM. *Acta Crystallogr. D Biol. Crystallogr.* **67,** 271–281
37. Evans, P. (2006) Scaling and assessment of data quality. *Acta Crystallogr. D Biol. Crystallogr.* **62,** 72–82
38. Adams, P. D., Afonine, P. V., Bunkóczi, G., Chen, V. B., Davis, I. W., Echols, N., Headd, J. J., Hung, L. W., Kapral, G. J., Grosse-Kunstleve, R. W., McCoy, A. J., Moriarty, N. W., Oeffner, R., Read, R. J., Richardson, D. C., Richardson, J. S., Terwilliger, T. C., and Zwart, P. H. (2010) PHENIX: a comprehensive Python-based system for macromolecular structure solution. *Acta Crystallogr. D. Biol. Crystallogr.* **66,** 213–221
39. Emsley, P., Lohkamp, B., Scott, W. G., and Cowtan, K. (2010) Features and development of Coot. *Acta Crystallogr. D. Biol. Crystallogr.* **66,** 486–501
40. Joosten, R. P., Joosten, K., Murshudov, G. N., and Perrakis, A. (2012) PDB_REDO: constructive validation, more than just looking for errors. *Acta Crystallogr. D Biol. Crystallogr.* **68,** 484–496
41. Saridakis, E., and Chayen, N. E. (2000) Improving protein crystal quality by decoupling nucleation and growth in vapor diffusion. *Protein Sci.* **9,** 755–757
42. Alexander-Miller, M. A., Parker, K. C., Tsukui, T., Pendleton, C. D., Coligan, J. E., and Berzofsky, J. A. (1996) Molecular analysis of presentation by HLA-A2.1 of a promiscuously binding V3 loop peptide from the HIV-envelope protein to human cytotoxic T lymphocytes. *Int. Immunol.* **8,** 641–649
43. Georgiadou, D., Hearn, A., Evnouchidou, I., Chroni, A., Leondiadis, L., York, I. A., Rock, K. L., and Stratikos, E. (2010) Placental leucine aminopeptidase efficiently generates mature antigenic peptides *in vitro* but in patterns distinct from endoplasmic reticulum aminopeptidase 1. *J. Immunol.* **185,** 1584–1592
44. Liao, S. M., Du, Q. S., Meng, J. Z., Pang, Z. W., and Huang, R. B. (2013) The multiple roles of histidine in protein interactions. *Chem. Cent. J.* **7,** 44
45. Hattori, A., Goto, Y., and Tsujimoto, M. (2012) Exon 10 coding sequence is important for endoplasmic reticulum retention of endoplasmic reticulum aminopeptidase 1. *Biol. Pharm. Bull.* **35,** 601–605
46. Hisatsune, C., Ebisui, E., Usui, M., Ogawa, N., Suzuki, A., Mataga, N., Takahashi-Iwanaga, H., and Mikoshiba, K. (2015) ERp44 exerts redox-dependent control of blood pressure at the ER. *Mol. Cell* **58,** 1015–1027
47. Aldhamen, Y. A., Pepelyayeva, Y., Rastall, D. P., Seregin, S. S., Zervoudi, E., Koumantou, D., Aylsworth, C. F., Quiroga, D., Godbehere, S., Georgiadis, D., Stratikos, E., and Amalfitano, A. (2015) Autoimmune disease-associated variants of extracellular endoplasmic reticulum aminopeptidase 1 induce altered innate immune responses by human immune cells. *J. Innate Immun.* **7,** 275–289
48. Chang, S. C., Momburg, F., Bhutani, N., and Goldberg, A. L. (2005) The ER aminopeptidase, ERAP1, trims precursors to lengths of MHC class I peptides by a "molecular ruler" mechanism. *Proc. Natl. Acad. Sci. U.S.A.* **102,** 17107–17112
49. Gandhi, A., Lakshminarasimhan, D., Sun, Y., and Guo, H. C. (2011) Structural insights into the molecular ruler mechanism of the endoplasmic reticulum aminopeptidase ERAP1. *Sci. Rep.* **1,** 186
50. Infantes, S., Samino, Y., Lorente, E., Jiménez, M., García, R., Del Val, M., and López, D. (2010) Cutting edge: H-2L(d) class I molecule protects an HIV N-extended epitope from *in vitro* trimming by endoplasmic reticulum aminopeptidase associated with antigen processing. *J. Immunol.* **184,**

3351–3355
51. Kanaseki, T., Blanchard, N., Hammer, G. E., Gonzalez, F., and Shastri, N. (2006) ERAAP synergizes with MHC class I molecules to make the final cut in the antigenic peptide precursors in the endoplasmic reticulum. *Immunity* **25,** 795–806
52. Hammer, G. E., Gonzalez, F., Champsaur, M., Cado, D., and Shastri, N. (2006) The aminopeptidase ERAAP shapes the peptide repertoire displayed by major histocompatibility complex class I molecules. *Nat. Immunol.* **7,** 103–112
53. Blanchard, N., Kanaseki, T., Escobar, H., Delebecque, F., Nagarajan, N. A., Reyes-Vargas, E., Crockett, D. K., Raulet, D. H., Delgado, J. C., and Shastri, N. (2010) Endoplasmic reticulum aminopeptidase associated with antigen processing defines the composition and structure of MHC class I peptide repertoire in normal and virus-infected cells. *J. Immunol.* **184,** 3033–3042

Immunology:

Structural Basis for Antigenic Peptide Recognition and Processing by Endoplasmic Reticulum (ER) Aminopeptidase 2

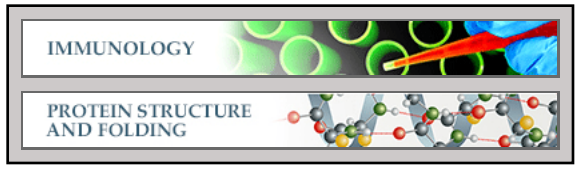

Anastasia Mpakali, Petros Giastas, Nikolas Mathioudakis, Irene M. Mavridis, Emmanuel Saridakis and Efstratios Stratikos

J. Biol. Chem. 2015, 290:26021-26032.
doi: 10.1074/jbc.M115.685909 originally published online September 17, 2015
